Interactions leading to disordered ground states and unusual low-temperature behavior

Robert D. Batten,[1] Frank H. Stillinger,[2] and Salvatore Torquato[2,3,4,5,6,*]
[1]*Department of Chemical Engineering, Princeton University, Princeton, New Jersey 08544, USA*
[2]*Department of Chemistry, Princeton University, Princeton, New Jersey 08544, USA*
[3]*Princeton Materials Institute, Princeton University, Princeton, New Jersey 08544, USA*
[4]*Program in Applied and Computational Mathematics, Princeton University, Princeton, New Jersey 08544, USA*
[5]*Princeton Center for Theoretical Science, Princeton University, Princeton, New Jersey 08544, USA*
[6]*School of Natural Sciences, Institute for Advanced Study, Princeton, New Jersey 08544, USA*
(Received 3 July 2009; published 4 September 2009)

We have shown that any pair potential function $v(r)$ possessing a Fourier transform $V(k)$ that is positive and has compact support at some finite wave number K yields classical disordered ground states for a broad density range [R. D. Batten, F. H. Stillinger, and S. Torquato, J. Appl. Phys. **104**, 033504 (2008)]. By tuning a constraint parameter χ (defined in the text), the ground states can traverse varying degrees of local order from fully disordered to crystalline ground states. Here, we show that in two dimensions, the "k-space overlap potential," where $V(k)$ is proportional to the intersection area between two disks of diameter K whose centers are separated by k, yields anomalous low-temperature behavior, which we attribute to the topography of the underlying energy landscape. At $T=0$, for the range of densities considered, we show that there is continuous energy degeneracy among Bravais-lattice configurations. The shear elastic constant of ground-state Bravais-lattice configurations vanishes. In the harmonic regime, a significant fraction of the normal modes for both amorphous and Bravais-lattice ground states have vanishing frequencies, indicating the lack of an internal restoring force. Using molecular-dynamics simulations, we observe negative thermal-expansion behavior at low temperatures, where upon heating at constant pressure, the system goes through a density maximum. For all temperatures, isothermal compression reduces the local structure of the system unlike typical single-component systems.

DOI: 10.1103/PhysRevE.80.031105 PACS number(s): 05.20.−y, 82.35.Jk, 82.70.Dd, 61.50.Ah

I. INTRODUCTION

Soft-matter systems including colloids, microemulsions, and polymers are effectively modeled using simple soft pair interactions [1]. A soft interaction pair potential $v(r)$ is bounded and absolutely integrable, and typically short-ranged and repulsive [2]. Despite the simplicity of soft interactions, they give rise to a plethora of fascinating physical phenomena. For example, the Gaussian core potential, a theoretically appropriate model for polymer interactions [3], shows re-entrant melting and novel solid-solid and solid-fluid phase transitions [4–7] and exhibits negative thermal expansion (NTE) [8] and counterintuitive higher-dimensional behavior [9,10]. Other examples of soft interactions include a penetrable-sphere model that produces local clustering [11], the quadratic potential as used in dissipative particle dynamics [12], and an ultrasoft logarithmically divergent potential used as a model for star polymer solutions [13]. Additionally, soft pair interactions are easier to treat theoretically due to the finite energy at $r=0$ [2,14]. Duality relations linking properties of lattices to those of their dual lattices have been derived for the ground-state energies and elastic constants of the Gaussian core model [15,16] and for the ground-state energies of a general class of soft pair potentials [2].

Recently, a new class of soft pair potential functions has been of interest because the minimum potential energy configurations, or classical ground states, are disordered for a broad range of densities [17–20]. This class of pair potential functions includes any $v(r)$ with a Fourier transform $V(k)$ that is positive, bounded, and has compact support at some finite wave number K. For these $V(k)$, the corresponding $v(r)$ are generally long ranged and oscillatory. In previous work, the structural order in ground-state configurations, from disordered to crystalline structures, has been characterized [2,17–20]. More recently, this class of pair potential functions was used to design disordered ground-state configurations with targeted scattering characteristics [20] as part of a broader program of inverse statistical mechanical methods (see Ref. [21] and references therein).

Considering the counterintuitive structure of the ground states, we seek to explore the excited-state ($T>0$) properties of such systems in two dimensions using the "k-space overlap potential" as our model potential, which is detailed in Sec. II. For this potential, $V(k)$ is proportional to the intersection area between two disks of diameter K whose centers are separated by k [2]. It is also the Fourier-space analog of a real-space "overlap" potential that arises in connection with local-density fluctuations in point patterns [22].

We intend to shed light on the underlying energy landscape that is responsible for classical disordered ground states and certain ground-state and positive-temperature properties. We focus our attention on two dimensions because it is computationally more efficient and easier to visualize than three dimensions. However, for the more general compact-support class of $V(k)$, anomalous ground-state behavior can be found in one, two, and three spatial dimensions. For example, in one dimension, ground states undergo

*Corresponding author. torquato@electron.princeton.edu

an infinite number of "phase transitions" across the entire density range as ground states switch between Bravais and non-Bravais lattices [2,23].

We have briefly outlined the salient components of this study in a Letter [24]. In this paper, we not only expand on this previous work but we also provide additional results regarding the degeneracy of properties for ground-state lattice structures, the equation of state, and structural changes at positive temperature, as well as comprehensive discussion of these unusual behaviors. Specifically, we use lattice sums to show the continuous degeneracy of thermodynamic properties at $T=0$ for the family of rhombical Bravais lattices and the effect on the shear moduli over the relevant density range. Further, an analysis of normal modes provides an understanding the relative mechanical stability of lattice and disordered structures in the harmonic regime. Lastly, molecular-dynamics simulations are used to find the equation of state and structural order for various pressures and positive temperatures. We find a number of unusual properties including maximal Poisson's ratio of unity, vanishing normal-mode frequencies, and negative thermal expansion. These anomalous properties are attributed to the nontrivial topographic features of the energy landscape.

The remainder of this paper is as follows. In Sec. II, we provide mathematical preliminaries and review some general features of the ground-state properties, while the overlap potential is introduced in Sec. III. The various methods utilized in this study are found in Sec. IV. Section V details the normal modes (i.e., harmonic behavior) for various densities. The ground-state properties of lattice structures, with particular emphasis on the triangular lattice, are detailed in Sec. VI. In Sec. VII, we examine the results of molecular-dynamics simulations—the equation of state and thermodynamic and structural characteristics at various temperatures and pressures. Lastly, a discussion of these results, including their connection to the energy landscape, is found in Sec. VIII.

II. COLLECTIVE COORDINATES

A. Mathematical relations

For a system of N identical particles within a volume Ω with positions $\mathbf{r}_i$ that interact via pairwise additive potential $v(r)$, the total potential energy is given by

$$\Phi = \sum_{i<j} v(r_{ij}), \tag{1}$$

where $r_{ij} \equiv |\mathbf{r}_i - \mathbf{r}_j|$. Periodic boundary conditions and the minimum image convention are employed here. A subset of pair potential functions will now be identified for use in the following which includes those $v(r)$ that are bounded and absolutely integrable such that their Fourier transforms $V(k)$ exist for all wave vectors k. The Fourier transform pair satisfies

$$v(\mathbf{r}) = \frac{1}{\Omega}\sum_{\mathbf{k}} V(\mathbf{k})\exp(-i\mathbf{k}\cdot\mathbf{r}), \tag{2}$$

$$V(\mathbf{k}) = \int_{\Omega} v(\mathbf{r})\exp(i\mathbf{k}\cdot\mathbf{r})d\mathbf{r}, \tag{3}$$

where the summation covers an infinite number of wave vectors. In the infinite-volume limit, the pair potential function and its Fourier transform are isotropic so that the relevant variables for $v(\mathbf{r})$ and $V(\mathbf{k})$ are $r \equiv |\mathbf{r}|$ and $k \equiv |\mathbf{k}|$, respectively. The appropriate wave vectors for a region of space with dimensions $L_x \times L_y$ have components

$$\mathbf{k} = \left[\frac{2\pi n_x}{L_x}, \frac{2\pi n_y}{L_y}\right]. \tag{4}$$

The N-particle system potential energy is equivalently represented by

$$\Phi = \frac{1}{2\Omega}\sum_{\mathbf{k}} V(\mathbf{k})[\rho(\mathbf{k})\rho(-\mathbf{k}) - N] \tag{5}$$

$$= \frac{1}{\Omega}\sum_{\mathbf{k}} V(\mathbf{k})C(\mathbf{k}), \tag{6}$$

where the collective coordinates $\rho(\mathbf{k})$ are the Fourier coefficients of the density field and $C(\mathbf{k})$ is a related real-valued function

$$\rho(\mathbf{k}) = \sum_{j=1}^{N} \exp(i\mathbf{k}\cdot\mathbf{r}_j) \tag{7}$$

and

$$C(\mathbf{k}) = \sum_{i<j} \cos[\mathbf{k}\cdot(\mathbf{r}_j - \mathbf{r}_i)]. \tag{8}$$

The collective coordinates also convey structural information through the structure factor $S(\mathbf{k})$ and the pair distribution function $g_2(\mathbf{r})$ via

$$S(\mathbf{k}) = \frac{\langle|\rho(\mathbf{k})|^2\rangle}{N}, \tag{9}$$

where $\langle\cdots\rangle$ is the ensemble average and, omitting the $\mathbf{k}=0$ wave vector,

$$S(\mathbf{k}) = 1 + \rho\int \exp(i\mathbf{k}\cdot\mathbf{r})[g_2(\mathbf{r}) - 1]d\mathbf{r}, \tag{10}$$

where ρ is the number density N/Ω. Fan *et al.* [17] provided additional basic identities and inequalities regarding $\rho(\mathbf{k})$ and $C(\mathbf{k})$.

B. Ground states

By limiting the set of $v(r)$ to those with $V(k)$ that are positive, bounded, and have compact support at wave number K, ground states can be constructed by numerical optimization [17–20] and the ground-state properties are more amenable to theoretical analysis [2,14,25]. Given that $V(k)$ is positive and that the minimum value of $C(\mathbf{k})$ is $-N/2$, it is clear that any configuration in which the $C(\mathbf{k})$'s are constrained to their minimum value for all $0 < |\mathbf{k}| \leq K$ is a

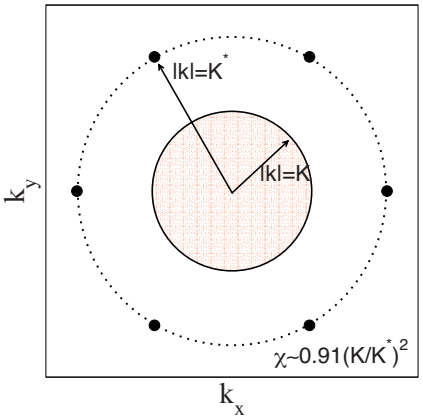

FIG. 1. (Color online) Structure factor for the triangular lattice. The black dots indicate the location of the first Bragg peaks. The constrained area of k space (shaded) cannot exceed the total area enclosed by the dotted circle. The value of χ is approximately $0.91(K/K^*)^2$.

ground-state configuration. We use $\mathbf{Q}$ to represent the set of wave vectors centered spherically about the origin for which $0<|\mathbf{k}|\leq K$. By Eq. (6), it is obvious that a ground-state configuration (global minimum potential energy) is one in which

$$\Phi = \frac{V(0)C(0)}{\Omega} - \left(\frac{N}{2\Omega}\right)\sum_{\mathbf{k}\in\mathbf{Q}} V(\mathbf{k}) \tag{11}$$

if all $C(\mathbf{k})$ for $|\mathbf{k}|$ in $\mathbf{Q}$ are simultaneously minimized. Note that the $\mathbf{k}=\mathbf{0}$ wave vector contributes a structure-independent constant to the potential energy.

For a fixed number density ρ, K must be less than K^* in order to construct a ground state by numerical optimization, where K^* is at the first Bragg peak associated with certain Bravais lattices. Sütő showed that these lattices are the integer, triangular, and body-centered cubic lattices in one, two, and three dimensions, respectively, and he also provided the relation between ρ and K^* for which these lattices are unique ground states [14]. With $K>K^*$, any attempt to construct a ground state will suppress the Bragg peak of the lattice and in doing so, $C(K^*)$ and other $C(\mathbf{k})$'s cannot simultaneously be minimized to $-N/2$. Thus Eq. (11) fails to hold and the ground states for $K>K^*$ are unknown.

In describing these systems, it is often useful to refer to the dimensionless parameter

$$\chi = \frac{M(K)}{dN} \tag{12}$$

as the fraction of degrees of freedom that are constrained, where $M(K)$ is the number of independent wave vectors in the set $\mathbf{Q}$ and dN is the total number of degrees of freedom [18]. We have constructed ground states in one [17], two [18,20], and three [19,20] dimensions via numerical optimization for various values of χ ranging from 0 to χ^*. The value of χ^* is dimension-dependent and corresponds to K^*. We limit our study to those systems for which $K<K^*$, equivalently $\chi<\chi^*$. Since $\chi^*=0.91$ in two dimensions, χ is approximately equal to the ratio of the area defined by $\mathbf{Q}$ relative to the circular area of k space defined by K^*, [i.e., $\chi\approx 0.91(K/K^*)^2$]. This is illustrated in Fig. 1.

By varying χ though all acceptable values, numerical optimization procedures identify distinct classes of structural order. In one and two dimensions, three distinct classes of ground-state structures arise. A disordered structure is one in which constraining $C(\mathbf{k})$ to be minimal for wave vectors in $\mathbf{Q}$ does not implicitly minimize $C(\mathbf{k})$ outside of $\mathbf{Q}$. The second class of structures, for $d=2$ defined as wavy crystalline, comprises those ground states in which constraining $C(\mathbf{k})$ to be minimal for all $\mathbf{k}$ in $\mathbf{Q}$ implicitly minimizes some $C(\mathbf{k})$ for $\mathbf{k}$ outside of $\mathbf{Q}$. In one dimension, this k-space structure gives rise to a particular sequence in the spacing of minimal and nonminimal $C(\mathbf{k})$ [17]. In two dimensions, the wavy r-space crystalline structure appears as a nonuniformly sheared triangular or square lattice [18]. The distinction between disordered and wavy crystallines is a mathematical definition concerning the $C(\mathbf{k})$'s and is not a physical phase transition. In the third class, numerical optimization procedures were only able to identify certain crystalline ground states. For these last structures, all $C(\mathbf{k})$ are minimized except those associated with Bragg scattering [17,18]. In three dimensions, disordered and crystalline regions were identified but no analogous wavy-crystalline region was found [19]. Table I summarizes the approximate χ values for transitions between structural regions at ground state.

When exploring the thermal properties of the overlap potential, it is more natural to work with number density ρ instead of χ, as the length scale $1/K$ is fixed to unity. There is an inverse relation between χ and ρ. As χ goes to zero, the density approaches infinity. Table II shows the relation between χ and ρ with $K=1$ for ground-state regions and certain Bravais and non-Bravais lattice structures in $d=2$. The lattices are ground states for all χ less than the associated maximal χ. Note that the densities in the chart can be calculated exactly for lattices with $K=1$ [14]. Since we deal with finite systems, the distribution of the independent wave vectors can produce some variation in χ. Typically this variation is small. For example, converting $\rho=0.0253$ to χ gives values of 0.7799 and 0.7667 for 418 and 780 particles, respectively. In Table II, the χ values were estimated using systems containing 418 particles.

TABLE I. Structural regions for various χ and spatial dimension d.

d	Ref.	Disordered	Wavy Crystalline	Crystalline
1	[17]	$\chi\leq\frac{1}{3}$	$\frac{1}{3}<\chi<\frac{1}{2}$	$\frac{1}{2}\leq\chi\leq 1$
2	[18]	$\chi<0.57655$	$0.57655\leq\chi<0.77990$	$0.77990\leq\chi\leq 0.91$
3	[19]	$\chi\leq 0.50066$	No analog reported	$0.50066<\chi<0.98133$

TABLE II. Maximum χ values as estimated from systems containing 418 particles and the corresponding ρ for certain lattices and structural transitions for $K=1$.

	χ	$10^2\rho$
Infinite density "ideal-gas"	0	∞
Max. χ for kagomé lattice	0.30	6.57
Max. χ for honeycomb lattice	0.44	4.38
Disorder $\rightarrow$ wavy crystalline	0.58	3.46
Wavy crystalline $\rightarrow$ crystalline	0.78	2.53
Max. χ for square lattice	0.78	2.53
Max. χ for tri. lattice	0.91	2.19

III. OVERLAP POTENTIAL

The results reviewed above hold for any positive and bounded $V(k)$ that has compact support at K. This class of $V(k)$ generally produces a long-ranged $v(r)$ with oscillatory forces in the infinite-volume limit. We choose to probe the phase behavior for a specific pair potential function. Initially, a square-mound $V(k)$ was considered due to its simplicity. However, in the infinite-volume limit, the corresponding $v(r)$ is too long ranged and the pressure, as calculated by the virial theorem, diverges for large particle separations. To diminish the range of $v(r)$ and smooth out oscillations, we sought a $V(k)$ that went continuously to zero at K. Most $V(k)$, including $V(k) \propto (k-K)^\beta$ for positive β and truncation at K, do not produce simple analytic expressions for $v(r)$. We ultimately chose the overlap potential since its $v(r)$ is sufficiently damped and analytic expressions exist for both $V(k)$ and $v(r)$.

The k-space overlap potential, previously introduced as a real-space pair potential function that arises in connection to local-density fluctuations in point patterns [22], is proportional to the intersection area between two disks of diameter K whose centers are separated by k,

$$V(k) = \frac{2V_0}{\pi}\left[\cos^{-1}\left(\frac{k}{K}\right) - \frac{k}{K}\left(1-\frac{k^2}{K^2}\right)^{1/2}\right], \quad k \le K \tag{13}$$

and 0 otherwise, and in the infinite-volume limit, the pair potential function in r space is

$$v(r) = \frac{V_0}{\pi r^2}\left[J_1\left(\frac{Kr}{2}\right)\right]^2, \tag{14}$$

where J_1 is the first-order Bessel function. Figure 2 shows the pair potential function and its Fourier transform with $K=1$. The pair potential function $v(r)$ is bounded at $r=0$ and has small oscillatory features for large r. In the asymptotic large-r limit, the real-space pair potential function goes as

$$v(r) \sim \frac{4V_0}{K\pi^2 r^3}\cos^2\left(\frac{1}{2}Kr - \frac{3\pi}{4}\right). \tag{15}$$

The first minimum in the $v(r)$ occurs at $\frac{1}{2}Kr=3.8317$ and provides an effective diameter of $D^*=7.6634/K$ for these soft particles. For the rest of this paper, we will use dimensionless variables with the natural length $1/K$, energy V_0, and particle mass m taken to be unity.

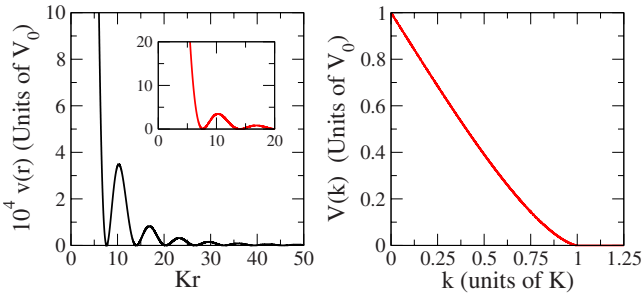

FIG. 2. (Color online) The pair potential function $v(r)$ and its Fourier transform, the overlap potential, $V(k)$.

Soft potentials are often adequate models for polymer systems and given the oscillatory nature of the overlap potential, it may be a reasonable model for special classes of polymers or colloids [21]. In a recent study, the average depletion force between two large colloids in semidilute polymer solutions was shown, by application of integral equations and molecular-dynamics simulations, to be oscillatory [26]. Therefore, it may be possible for the overlap potential to be an appropriate model for some colloidal systems although we are currently unaware if any such physical system has yet been examined experimentally.

In one dimension, it was shown that the ground states for the corresponding rod-rod overlap potential, as well as the Fourier transform of that overlap potential, undergo an infinite number of "phase transitions" between Bravais and non-Bravais lattices as the density is varied [2]. In two dimensions, we find that these long-ranged interactions, similar in form to Friedel oscillations in screened potentials of ions in molten metals [27], when applied to classical particles give rise to other unusual ground-state and thermal properties.

The maximum attainable χ in two dimensions is $\chi^*=0.91$ and with $K=1$, this corresponds to a density of $\rho^*=\frac{\sqrt{3}}{2(2\pi)^2} \approx 2.19\times 10^{-2}$, the number density of the reciprocal lattice of a close packing of disks in two dimensions. The range in which Eq. (11) applies is for $\chi \le 0.91$ and equivalently $\rho \ge \rho^*$.

IV. METHODS

A. Normal modes

Prior to this study, ground-state structures for $0 \le \chi \le \chi^*$ had been identified, but it was unknown whether these ground states were mechanically stable to thermal fluctuations. In the low-temperature limit, the potential energy is expanded about a global minimum to second order with respect to particle positions. The harmonic equations of motion are constructed by using the expanded potential energy and applying Newton's second law. The solution to this set of equations for a given configuration gives rise to the normal modes of the system. The calculation of normal-mode frequencies for disordered systems follows that of Brillouin's analysis of wave propagation in periodic structures [28]. Since our systems possess periodic boundary conditions, the

calculation of the dynamical matrix is equivalent to the calculation of normal modes associated with infinite-wavelength phonons. In this case, the dynamical matrix is simply the Hessian of the potential energy with respect to particle coordinates. The eigenvalues of the Hessian are the square of the normal-mode frequencies and the eigenvectors are the associated multidimensional directions of the modes.

If the frequencies of all modes are real and nonzero (i.e., the squares of the frequencies are positive), the particles undergo stable oscillations about their equilibrium position. If any mode frequency is imaginary, the system is unstable and is driven away from its initial state. However, if a mode frequency vanishes, then the configuration can be perturbed along the eigenvector direction without energy cost. For configurations with a vanishing frequency, in the vicinity of a global energy minimum, many directions in the energy landscape are uphill (the mode frequency is real and nonzero), but for other directions the energy landscape is flat (vanishing normal-mode frequency). A normal mode with a nonvanishing, real frequency actively contributes to the excess heat capacity, however, a zero-frequency mode does not. When heating a system, on average, the potential energy will respond linearly with the temperature of the system via equipartition with a slope proportional to the fraction of frequencies that are real and nonvanishing.

Consequently, we use the fraction of normal modes whose frequencies are real and nonvanishing as a quantitative characteristic of the energy landscape and a measure of the mechanical stability of a system. For a system under periodic boundary conditions in two dimensions, two mode frequencies will vanish corresponding to overall translation of the system, while the remaining $(2N-2)$ modes determine the stability characteristics of the system.

B. Ground-state properties

In Sec. VI, we make use of lattice sums and basic thermodynamic relations to explore the potential energy, pressure, isothermal compressibility, Poisson's ratio, and elastic constants. The pair potential $v(r)$, Eq. (14), is utilized in the lattice sums and is truncated at several thousand unit cells from the origin so that finite-size effects are negligible.

The potential energy per particle for any Bravais lattice is

$$\phi = \Phi/N = \frac{1}{2}\sum_i v(|\mathbf{r}_i|), \tag{16}$$

where the summation is over all lattice sites $\mathbf{r}_i$, omitting the particle at the origin. The pressure, at zero temperature, is

$$p = -\frac{d\phi}{da} = -\frac{1}{4a}\sum_i |\mathbf{r}_i| v'(|\mathbf{r}_i|), \tag{17}$$

where $a=\rho^{-1}$ is the area per particle. The isothermal compressibility κ_T is related to the pressure via the expression

$$\frac{1}{\kappa_T} = -a\frac{dp}{da} = \frac{1}{8a}\sum_i [|\mathbf{r}_i|^2 v''(|\mathbf{r}_i|) - |\mathbf{r}_i| v'(|\mathbf{r}_i|)]. \tag{18}$$

For an isotropic structure in two dimensions, the Poisson's ratio is given by

$$\nu_{tri} = \frac{2\lambda_{xyxy} - \lambda_{xxyy}}{2\lambda_{xyxy} + \lambda_{xxyy}}, \tag{19}$$

where λ_{xyxy} is the elastic constant for isotropic compression and λ_{xxyy} is that for the uniform strain in one direction and a subsequent uniform strain in the perpendicular direction [29]. The elastic constants can be written in terms of the pair potential function

$$\lambda_{xyxy} = \frac{1}{32a}\sum_i [|\mathbf{r}_i|^2 v''(|\mathbf{r}_i|) - |\mathbf{r}_i| v'(|\mathbf{r}_i|)], \tag{20}$$

$$\lambda_{xxyy} = \frac{1}{4a}\sum_i \left[\left(\frac{x_i^2 y_i^2}{|\mathbf{r}_i|^2} \right) v''(|\mathbf{r}_i|) + \left(\frac{|\mathbf{r}_i|}{2} - \frac{x_i^2 y_i^2}{|\mathbf{r}_i|^3} \right) v'(|\mathbf{r}_i|) \right], \tag{21}$$

as was displayed previously [30]. Note that λ_{xyxy} is simply $1/\kappa_T$. The results of these calculations reveal much about the crystalline ground-state regime and the continuous energy degeneracy among lattice structures.

C. Molecular dynamics methods

Molecular dynamics methods were used to determine the equilibrium structural and thermodynamic properties at positive temperature for the density range $\rho \geq \rho^*$ (i.e., $\chi \leq 0.91$). The potential energy and forces were calculated using Eq. (5) as opposed to Eq. (6) since time-saving trigonometric identities can be employed. The equations of motion were integrated using the velocity-Verlet algorithm [31] with a time step of 0.4, chosen so that energy was accurately conserved when integrating the equations of motion in the *NVE* ensemble. Periodic boundary conditions were employed using a square simulation box.

Constant density simulations were performed in the *NVT* ensemble by employing an Andersen thermostat [32]. Systems contained either 418 or 780 particles and were initialized in a triangular lattice, slightly strained to fit in the square box [33]. When constructing the equation of state, the systems of 418 particles were equilibrated for at least 200 000 time steps before sampling properties for an additional 200 000 time steps. Systems of 780 particles were equilibrated for at least 50 000 time steps and properties were averaged over an additional 30 000 time steps. In this study, we observe no significant differences in the equilibrium properties at positive temperature between these modest system sizes. Increasing the system size well beyond 780 particles is currently too computationally intensive considering the nature of the potential and the size scaling of Eq. (5). We also used molecular dynamics to estimate the fraction of normal modes that have nonvanishing, real frequencies by the slope of the equilibrium $\phi - T$ curve in the low-temperature region.

Constant pressure simulations were performed in the *NPT* ensemble by using a scheme that couples molecular dynamics with Monte Carlo volume sampling [34]. The equations of motion were integrated as usual with the Andersen thermostat. After each time step, a random, isotropic volume move was attempted and accepted with the probability

$$P(\Delta V) = \min[1, \exp(-\{\Delta\Phi + p_0 \Delta V - NkT_0 \ln[(V+\Delta V)/V]\}/kT_0)], \quad (22)$$

where p_0 and T_0 are the imposed pressure and temperature and $\Delta\Phi$ and ΔV are the differences between the trial move and the original potential energy and volume. This method was preferred over extended Lagrangian methods since this does not require calculation of the virial at each time step. The calculation of the internal virial requires explicit calculation of pair forces via Eqs. (6) and (8) and scales poorly with the number of particles. Thus, in order simulate longer times, it was best to avoid calculation of the virial at every time step. The calculation of total forces on particles as required for integrating the equations of motion is simpler using Eq. (5) and suitable trigonometric identities. The systems were initialized in the triangular lattice at $\rho=\rho^*$ and the volume was rescaled, similar to that of the Berendsen barostat [35], so as to start the simulation near the target pressure. If the pressure drifted significantly during the equilibration period, the volume was rescaled until the pressure settled about the target pressure.

Additionally, systems initialized in the triangular lattice were slowly heated (at constant pressure or constant density) and the resulting systems were then slowly cooled to nearly zero temperature to observe hysteresis effects. It is important to note that in the *NVT* ensemble, χ is a fixed parameter and in the *NPT* ensemble, χ fluctuates, so that it is necessary to adjust χ after every accepted volume change.

V. RESULTS: NORMAL MODES

The parameter χ originally was introduced to represent the fraction of degrees of freedom that are constrained [18]. Since the fraction of modes with nonzero, real frequencies is indicative of the relative number of constrained degrees of freedom, one might expect the fraction of normal modes with nonvanishing, real frequencies to equal χ.

For example, for a system with no imposed constraints, $\chi=0$, all eigenvalues of the dynamic matrix are identically zero since there are no interactions. For each constraint imposed upon the system [i.e., forcing $C(\mathbf{k})$ to be minimal for some $\mathbf{k}$], one might expect exactly one mode's frequency to switch from vanishing to nonzero and real while all others remain zero if the constraints are independent. However, we find that for $\chi<0.5$, constraining one independent wave vector $\mathbf{k}$ results in the switching of two frequencies from vanishing to nonzero and real. Figure 3 shows the fraction of modes in which in the frequencies are vanishing as a function of χ. The slope in the linear part is *exactly* −2. The two-to-one relation comes about simply from the fact that constraining $C(\mathbf{k})$ to be minimal is equivalent to constraining $|\rho(\mathbf{k})|$ to be zero and consequently one requires that

$$\sum_{i=1}^{N} \sin(\mathbf{k}\cdot\mathbf{r}_i) = 0 \quad (23)$$

and

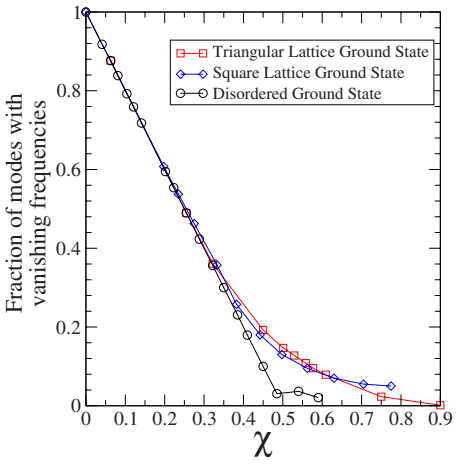

FIG. 3. (Color online) Fraction of normal modes with vanishing frequency as a function of χ for disordered and ordered structures as calculated for $N=780$. The slope in the linear part is exactly −2.

$$\sum_{i=1}^{N} \cos(\mathbf{k}\cdot\mathbf{r}_i) = 0. \quad (24)$$

These constraints are apparently independent for $\chi<0.5$. Imposing that $C(\mathbf{k}_1)$ be minimal does not influence $C(\mathbf{k}_2)$ provided that $\mathbf{k}_1$ is within the radial cutoff K associated with $\chi=0.5$ and $\mathbf{k}_2$ is outside of K.

In the region $0.5<\chi\leq 0.78$, for disordered and wavy-crystalline structures, nearly all of the mode frequencies are real and nonzero. For these calculations, several representative ground-state configurations were used and between 92%–98% of the frequencies were nonzero and real while all others were zero. The square lattice and triangular lattice have more vanishing frequencies than disordered ground states for $\chi>0.3$. Lattice structures, surprisingly, have as many as 12% more vanishing frequencies than nonlattice structures when compared at the same χ, implying that lattices are mechanically less stable than their disordered counterparts.

For the triangular lattice at its maximum attainable $\chi=0.91$, exactly two mode frequencies vanish (for overall translation in $d=2$). Thus the only ground state is the triangular lattice, a two-dimensional manifold in the energy landscape (aside from particle permutations). By compressing the system, effectively decreasing χ, the energy landscape develops channels of depth equal to the global energy minimum running through the triangular lattice. These channels are evidenced by the vanishing normal-mode frequencies and represent the presence of energetically degenerate configurations. Upon further compression so that $\chi<0.5$, even disordered ground states have many directions in the energy landscape that are absolutely flat. Continuous perturbations from these points can take the system from one ground state to another energetically degenerate ground state without energy cost. We discuss the topography of the energy landscape further in Sec. VIII.

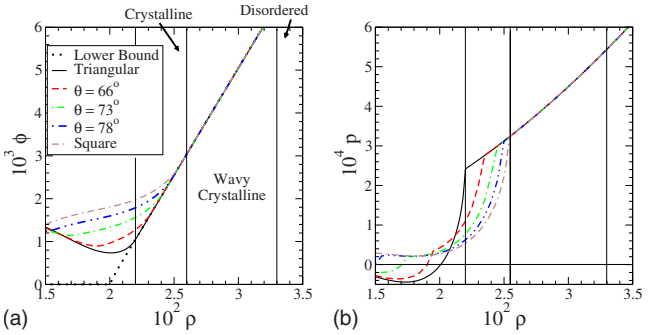

FIG. 4. (Color online) (a) Lattice sums and (b) pressure at $T=0$ for the rhombical Bravais lattices with the overlap potential. The triangular lattice is a ground state for $\rho \geq 2.19 \times 10^{-2}$, the square lattice and wavy-crystalline structures are ground states for $\rho \geq 2.52 \times 10^{-2}$, and certain disordered structures are ground states for $\rho \geq 3.30 \times 10^{-2}$.

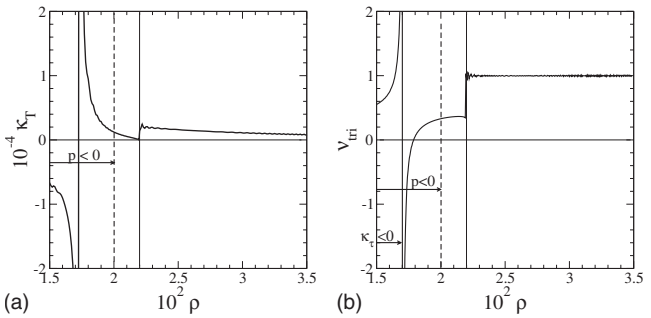

FIG. 5. (a) Isothermal compressibility of the triangular lattice interacting via the overlap potential. A region left of the dashed line corresponds to negative pressure. (b) Poisson's ratio for the triangular lattice interacting via the overlap potential. Above ρ^*, the Poisson's ratio is unity.

VI. RESULTS: MACROSCOPIC BEHAVIOR OF LATTICE GROUND STATES

A. Lattice sums

Lattice sums were performed for the family of rhombical Bravais lattices. Varying the angle between the lattice vectors allowed for investigation of all rhombical lattices between the triangular lattice and square lattice. This calculation confirms that the triangular lattice is indeed the ground state for the largest density range, for $\rho \geq \rho^*$, as shown in Fig. 4(a).

The square lattice is part of the degenerate ground state for densities $\rho \geq 2.53 \times 10^{-2}$ ($\chi \leq 0.78$), which is also the value that was previously identified as the transition between wavy-crystalline and crystalline ground states. In light of these observations, it may be possible to consider the wavy-crystalline ground state as the manifestation of the union of Bravais lattices described for this class of potentials [14]. This coexistence of lattice configurations, as in the wavy-crystalline and disordered regions, suggests that lattice structures are distinct global minima in the energy landscape that are connected to each other via continuous paths of depth equal to the global minimum potential energy.

Despite the existence of energy degenerate ground states for χ values in the crystalline region, numerical optimization techniques consistently found only the triangular lattice and no other lattice structures [18,20]. One might suggest that system geometry would favor the triangular lattice, since N was chosen to fit a triangular lattice in a square simulation box, or that the initial condition, a perturbed triangular lattice, biased the numerical optimization procedure. However, when using, say, $N-1$ or $N+1$ particles with a random initial condition, the system would attempt to form a triangular lattice by aligning particles locally with perfect sixfold symmetry but rotated uniformly to fit in the box and satisfy periodic boundary conditions. The optimization almost always gets trapped in a local energy minimum above the ground state when using random initial configurations. The local-minimum configuration usually resembled a triangular lattice with vacancy or grain-boundary defects and never resembled another lattice. Upon changing the simulation cell to a rhombus, the minimization procedure similarly favored the triangular lattice when $\chi=0.91$. At lower χ, applying minimization procedures to small, random perturbations from other rhombical lattices would return the system to the perfect lattice as a ground state. Further discussions of the energy landscape implications of this are relegated to Sec. VIII.

For the density range $\rho < \rho^*$, the ground states are not known. However, the minimum-energy Bravais-lattice structure provides an upper bound on the ground-state energy via appropriate duality relations [2] and on account of the nonnegativity of the pair potential function, $\phi=0$ is the lower bound. We have found at least local energy-minimizing structures whose energy falls within the bounds. These structures resemble a triangular lattice coexisting with a gas (void) phase and are at positive pressure. However, without application of Eq. (11), we cannot determine if these are true ground states and therefore this density region is not of relevance to this work.

B. Pressure, isothermal compressibility, and Poisson's ratio

Because the triangular lattice is unique among all disordered and lattice ground states, we investigated its macroscopic behavior. The pressure-density curve, Fig. 4(b), shows a distinct cusp despite that fact that the pair potential is continuous. The isothermal compressibility-density curve [Fig. 5(a)] is also discontinuous at ρ^* despite the continuous potential.

Each rhombical lattice has similar behavior due to the subtle change in curvature at its respective critical density. For $\rho > \rho^*$, the system becomes insensitive to the potential. This notion was suggested in earlier work by considering the energy of the dual lattice interacting with the dual potential [14]. As the density goes to infinity, the isothermal compressibility goes monotonically to zero. For some densities below ρ^*, the isothermal compressibility of the triangular lattice is negative and thus this lattice is mechanically unstable for those densities and can be ruled out as a potential ground state. For a fundamental cell with a multiparticle basis, the macroscopic behavior is similar to that of Bravais lattices, however, the corresponding densities for the discontinuities are much larger than those of rhombical Bravais lattices, as seen in Table II.

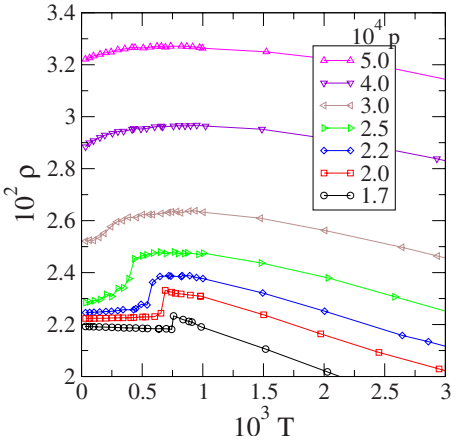

FIG. 6. (Color online) Density as function of temperature for several fixed pressures for 418 particles initialized as a triangular lattice and slowly heated. For $p > 1.7 \times 10^{-4}$, the systems show negative thermal expansion in the small-T region.

Because of the system's insensitivity to the pair potential function on the length scale of the particle at these densities, the Poisson's ratio for the triangular lattice [Fig. 5(b)] goes identically to unity for the entire density range $\rho > \rho^*$. Numerical error accounts for the small fluctuations about unity in the figure. The elastic constants are similarly discontinuous at ρ^*. As ρ approaches ρ^* from below, both the shear and isotropic elastic constant diverge to infinity. Above ρ^*, the shear elastic constant is identically zero and the isotropic elastic constant grows monotonically. The triangular lattice acts as an elastically incompressible material (i.e., on the macroscopic scale, deformations of the triangular lattice are volume preserving). The shear modulus goes to zero and the ratio of the shear to bulk modulus goes to infinity. These unusual properties are a consequence of the system being insensitive to the potential on these length scales.

VII. RESULTS: THERMAL BEHAVIOR

A. Equation of state and negative thermal expansion

The density equation of state, shown in Fig. 6, indicates that upon heating this system at constant pressure, for $p \geq 1.7 \times 10^{-4}$, the density goes through a maximum. Lower pressures were not considered since this caused χ to exceed 0.91 in the ground state. The thermal-expansion coefficient,

$$\alpha = -\frac{1}{\rho}\left(\frac{\partial \rho}{\partial T}\right)_p, \tag{25}$$

is negative for low temperatures. NTE is a physical phenomenon that can occur as a result of several mechanisms. In some cases, it arises due to an open, anisotropic crystalline structure collapsing upon melting, as is the case with water, and in other cases, the repulsive part of the pair potential function is tuned to coerce a crystal to densify upon heating [36]. However, the k-space overlap potential is isotropic and has attractive and repulsive forces. The mechanism for NTE in these systems shares some characteristics with that of the Gaussian core model (GCM). The GCM is a short-ranged,

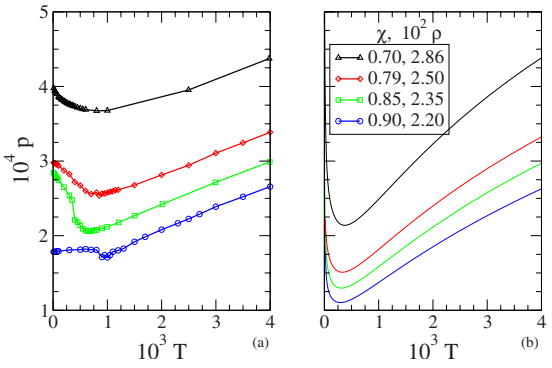

FIG. 7. (Color online) (a) Pressure equation of state for the overlap potential as calculated in the *NVT* ensemble containing 418 particles. (b) The virial equation of state truncated at the third virial coefficient always shows an initial drop in pressure upon heating.

soft-core pair potential that exhibits negative thermal expansion for a range of temperatures and densities [8]. In that model's mechanism, increases in the density "smooth" out the energy landscape in such a way that basins of attraction at higher ϕ flatten out faster upon compression than do basins of attraction at lower ϕ. Upon compression, systems at higher temperature do not increase potential energy as rapidly as systems at lower temperature, resulting in negative thermal expansion. In contrast to the GCM, it is the long-ranged and oscillatory nature of the k-space overlap potential which contributes to such a shape variation of the energy landscape.

NTE has a corresponding effect on the pressure equation of state. At $\rho = \rho^*$, the pressure increases initially and then has a discontinuous drop to a lower pressure. For densities greater than ρ^*, the pressure drop occurred immediately and smoothly decreased, achieving a minimum in the range $4 \times 10^{-4} \leq T \leq 8 \times 10^{-4}$. Due to the nonnegativity of the potential, low-order virial coefficients are positive and the system has no Boyle temperature. The virial equation of state truncated after third order in Fig. 7(b) predicts the qualitative decrease in pressure associated with negative thermal expansion. Given the effective diameter of particles, the system is at a relatively high density of soft particles and the virial equation of state is not expected to be quantitatively accurate in this density range

The potential energy always responds linearly with temperature in the harmonic region, which is typically in the range $T < 3 \times 10^{-4}$ for these systems. The initial slope of the potential energy-temperature curve for densities associated with the crystalline ground states $\rho^* \leq \rho \leq 2.53 \times 10^{-2}$ is unity as shown in Fig. 8. This is evidence that all of the normal modes (excepting those associated with overall translation) are actively contributing to the excess heat capacity. In Sec. V, direct calculation of the normal-mode frequencies indicated that the triangular lattice has several modes that do not actively contribute to the excess heat capacity. Upon addition of some thermal energies, the triangular lattice gets perturbed away from the lattice configuration in the energy landscape to a nearby configuration in which nearly all modes contribute to the excess heat capacity. Visual observation of the dynamics also reveals that the particles are not

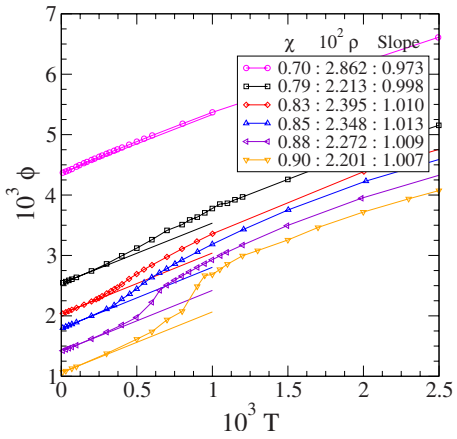

FIG. 8. (Color online) Potential energy per particle as a function of temperature at equilibrium as calculated in the *NVT* ensemble with a system containing 418 particles. The lines indicate the linear regression to the data in the harmonic region and the slope is indicated in the legend. The slopes of all the curves for small T are near unity.

necessarily oscillating about their initial lattice sites. For systems in which $\chi<0.5$, the initial slope of the $\phi-T$ curve was approximately 2χ as expected from the direct calculations in Sec. V. Also note from Fig. 8 that at all densities there is an inflection point in the $\phi-T$ curve indicating that the constant volume heat capacity achieves a maximum.

Heating and cooling cycles at constant pressure or constant density discover that hysteresis effects have strong density and pressure dependencies. For low pressures, these systems show a strong hysteresis effect that persists for $1.7\times10^{-4}\leq p<3.3\times10^{-4}$, but above this range the hysteresis effect disappears. Figure 9 shows the heating and cooling cycle for a system of 418 particles. The temperature was slowly increased in a stepwise fashion. The temperature was

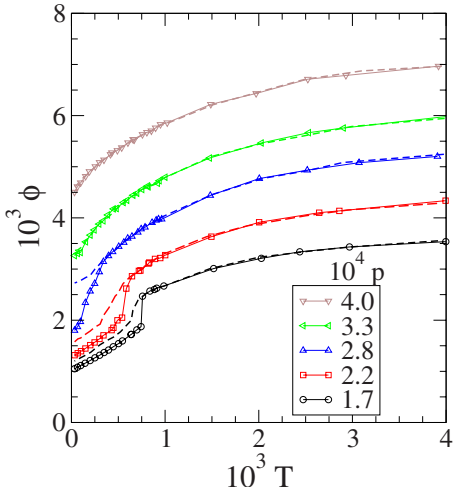

FIG. 9. (Color online) Hysteresis loops for a heating and cooling cycle starting with 418 particles in a triangular lattice at various pressures as indicated in the legend. Dashed lines indicate the cooling of a liquid while lines with data points indicate heating of the triangular lattice. At sufficiently high pressures, the heating and cooling curves are nearly identical, showing no hysteresis.

set to a target value, the system was left to equilibrate for a few thousand time steps, and then the temperature was increased to a new set point. Each data point represents the average value over a few hundred time steps at the respective temperature set point. A similar dependence on the extent of hysteresis exists for heating and cooling cycles at constant density. The hysteresis effect is strongest at low densities and eventually diminishes at higher densities. The lack of a hysteresis at high density and pressure suggests that the system does not get trapped in local energy minima in the cooling step.

B. Structural order

In the harmonic region at $\rho=\rho^*$, as T rises, particles oscillate about their lattice sites, a vacancy eventually appears, and a particle jumps from site to site. At high enough temperature, multiple vacancies build up and crystal melts to a liquid state. This progression is shown in the top row of Fig. 10 for $\rho=\rho^*$. However, for higher density, the transition is much less distinct. The middle and bottom rows of Fig. 10 show several snapshots of configurations for $\rho=2.35\times10^{-2}$ and 2.86×10^{-2} as systems undergo the transition from crystal to liquid. The middle row shows the system at $\rho=2.35\times10^{-2}$, $\chi=0.85$, in the harmonic region, near the melting point, and in the liquid state. The overall structure in the harmonic region appears to have wavy crystallinity and particles do not appear to oscillate about a lattice site. At the same temperature for even higher density, $\rho=2.86\times10^{-4}$, first image in the bottom row, the configuration from the harmonic region shows no memory of the initial lattice structure. There is clearly an excluded area around each particle center. In the high-temperature limit, the liquid states are disordered and visually similar to lower-density systems.

It is also interesting to note that in Fig. 10, there is no local nucleation or aggregation during a transition from crystal to disorder or during cooling. In some soft-matter systems, particles may cluster during cooling and form multioccupancy crystals [37]. Theoretical work suggests that the overlap potential is insufficient to form multioccupancy crystals in which some particles overlap with others to reduce the total potential energy [38,39]. A density-functional approach has also suggested this inability of the overlap potential to produce multioccupancy crystals [40]. Here, we do not observe nucleation when cooled as the attractive forces are apparently insufficient to promote local nuclei with six nearest neighbors. The transition from liquid to a crystal appears to be continuous as particles tend to "flow" into lattice sites.

We have also tracked changes in correlation functions with temperature and pressure by averaging over equilibrium molecular-dynamics trajectories. Figures 11 and 12 show the structure factors and radial distribution functions at low and high temperatures and several densities. With the relation between the potential energy, $V(k)$, and the structure factor, given in Sec. II, we can justify the shape of the structure factor at positive temperature. At the ground state, $S(k)$ is forced to zero for all $|\mathbf{k}|<K$. We observe that thermal energy is distributed according the weights upon which $V(k)$ "assigns" each $C(\mathbf{k})$ [and thus $S(k)$ for wave vectors $|\mathbf{k}|<K$].

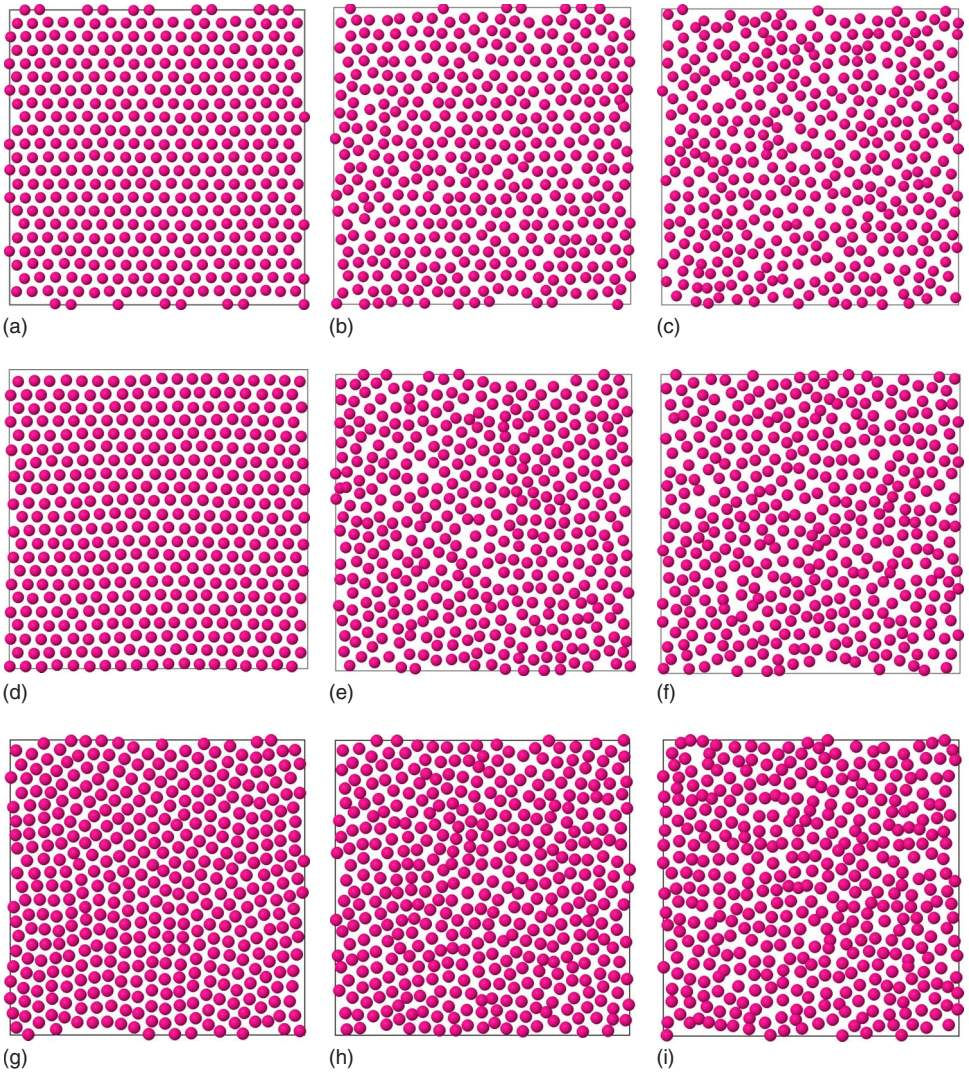

FIG. 10. (Color online) Snapshots of configurations. (Top row) $\rho=2.20\times10^{-2}$ ($\chi=0.91$), from left to right: $T\times10^3=0.1$, 0.7, and 1.0. (Middle row) $\rho=2.35\times10^{-2}$ ($\chi=0.85$), from left to right: $T\times10^3=0.1$, 0.7, and 1.0. (Bottom row) $\rho=2.86\times10^{-4}$ ($\chi=0.70$), from left to right: $T\times10^3=0.1$, 0.4, and 1.0. There is a lack of local nucleation and the transition from crystal to disorder appears to be first order only for $\rho=2.20\times10^{-2}$. Otherwise, the transition appears continuous. Particle sizes are chosen for clarity of the structure and are not reflective of the soft-core diameter.

Given that $V(k)$ is monotonically decreasing to zero at K, $V(k)$ assigns the least weight to large k and this is where we observe the most significant response in $S(k)$ with the application of thermal energy. Increases in the density smear out the $S(k)$ oscillations for k outside of the constraint radius K.

Upon the addition of thermal energy, the radial distribution function $g_2(r)$ smoothes out and at high-enough temperature, the particles are no longer surrounded by an effective hard core. For large r, there are oscillations in $g_2(r)$ with wavelengths of 2π that arise from the long-ranged oscillations of the pair potential function $v(r)$. Upon isothermal compression, neighbor peaks are smoothed out. These phenomena are strictly a characteristic of soft potential systems, as hard-core systems become locally more ordered with increasing density whereas soft-core particles experience increasing particle overlap.

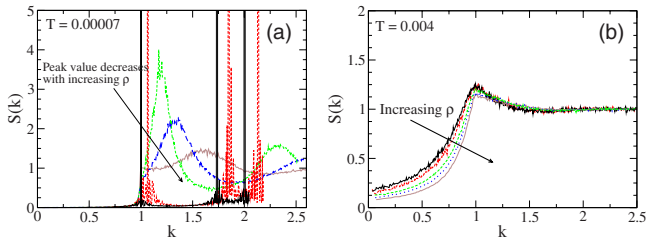

FIG. 11. (Color online) $S(k)$ for systems at $T=7\times10^{-5}$ (left) and 4×10^{-3} (right) and $\rho\times10^2=2.20$, 2.50, 3.31, 4.00, and 5.09 (equivalently, $\chi=0.90$, 0.79, 0.60, 0.50, and 0.40), averaged over many time steps for a system containing 418 particles. $S(k)$ for $\rho=2.20\times10^{-2}$ is truncated just past at $k=2$. It does not approach unity at $k=2$. Data were not collected for these k at $\rho=2.20\times10^{-2}$.

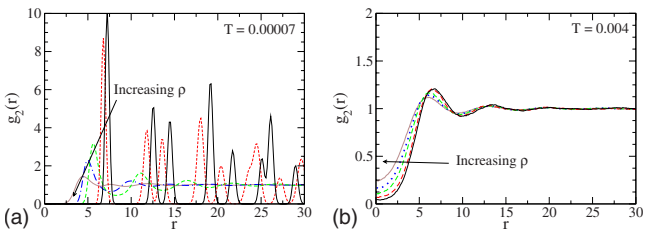

FIG. 12. (Color online) $g_2(r)$ (right) for systems at $T=7\times10^{-5}$ (left) and 4×10^{-3} (right) at $\rho\times10^2=2.20$, 2.50, 3.31, 4.00, and 5.09 (equivalently, $\chi=0.90$, 0.79, 0.60, 0.50, and 0.40), averaged over many time steps for a system containing 418 particles. Increases in density smooth out local order.

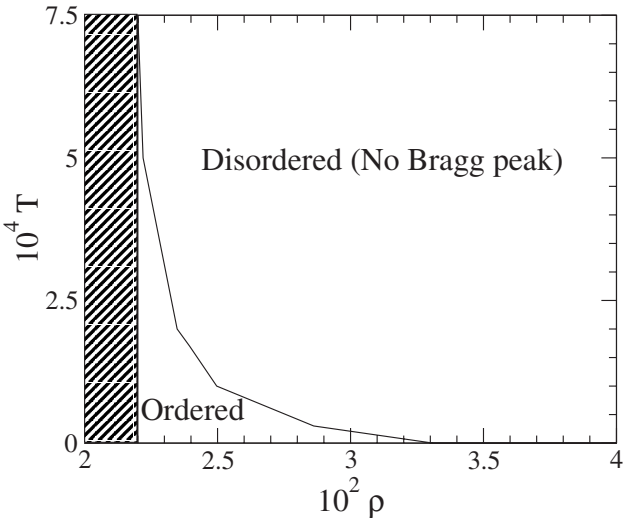

FIG. 13. An approximate structural phase diagram for the overlap potential. Within the ordered region, configurations have $S(k)$ with strong Bragg scattering characteristics. The disordered region does not show any strong Bragg scattering. Note that the ordered region includes wavy-crystalline ground states. The cross-hatched region represents $\chi > 0.91$, the region in which the ground states are unknown.

At low temperature and low density, Bragg scattering remains as observed in Fig. 11. Since Bragg scattering is evidence of long-ranged order, we have used this as a criterion to construct a structural phase diagram for the overlap potential. Figure 13 shows the density-temperature phase diagram. We define "ordered" states as those in which the first maximum of $S(k)$ is greater than 3. This is chosen so as to include the ground-state wavy crystal as an ordered state due to the perfect local coordination with slight harmonic distortion and effective hard core. As the density is increased, the temperature at which the Bragg scattering is destroyed sharply approaches zero. Densification of the system reduces the barriers in the energy landscape around the triangular lattice point so that only a small amount of thermal energy is required to destroy long-ranged order.

We have used the bond-orientational order parameter Ψ_6, defined as

$$\Psi_6 = \left| \frac{1}{N_{\text{bonds}}} \sum_j \sum_k e^{6i\theta_{jk}} \right|, \tag{26}$$

where θ_{jk} is the angle between two particles with respect to a fixed, but arbitrary, coordinate axis, to quantify the local hexatic order. The bond-orientational order parameter is an order metric where unity represents a perfect triangular lattice and zero represents no local hexatic order. An underlying triangular lattice is evident for $0.5 < \Psi_6 \leq 1$ where within the lower part of this range, the lattice is distorted by defects and fluctuations from the lattice sites. For a wavy-crystalline structure, Ψ_6 can range from about 0.4 to 0.8.

Figure 14 shows instantaneous values of Ψ_6 for various pressures upon slow heating. At the lowest pressure, $p = 1.7 \times 10^{-4}$, the bond order parameter gradually decreases and then shows a distinct drop at $T = 7.5 \times 10^{-4}$, signifying the loss of local order. This distinct drop also corresponds to the jump in density at this pressure. At higher pressures, the drop in the bond order parameter is less dramatic and has a more gradual decrease toward zero. At sufficiently high temperature, the order parameter drops and fluctuates below 0.1. Longer, near-equilibrium simulations for fixed NpT occasionally showed large fluctuations in the order parameter for $3.0 \times 10^{-4} < T < 6.0 \times 10^{-4}$ despite other state variables appearing well equilibrated, but generally showed significantly diminished local order. For $p < 2.3 \times 10^{-4}$, the equilibrium values show a distinct jump from high values to low values whereas at higher pressures they generally did not.

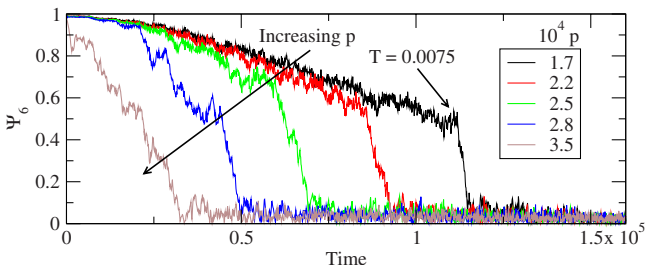

FIG. 14. (Color online) Instantaneous bond-orientational order parameter for various pressures for a system containing 418 particles heated at a linear rate of 7×10^{-8} temperature units per unit time. At low pressure, $p < 2.5 \times 10^{-4}$, the order parameter shows a sharp drop, indicative of a first-order phase transition. For higher pressures, the order parameter fluctuates and drops toward zero as the temperature is slowly increased.

Due to the sharp discontinuities associated with state variables at $\rho = \rho^*$ or the pressure p^* associated with ρ^* at zero temperature, the phase transition appears to be first order. For all densities greater than ρ^* or pressures above p^*, there is not necessarily a distinct jump in the thermodynamic quantities as the system transforms from crystalline to disordered. System size effects may be responsible for apparent lack of discontinuities for $\rho > \rho^*$ or $p > p^*$. However, given the degeneracy of ground states at all densities greater than ρ^*, it is likely that the phase transition is continuous for these densities. However, we have not fully investigated the nature of the phase transition since this is beyond the focus of the present work.

VIII. DISCUSSION

Systems of particles interacting via the overlap potential exhibit anomalous properties for densities greater than ρ^*. At the ground state, these systems exhibit energy degeneracy among Bravais-lattice structures and increases to the density bring about additional degeneracies with wavy-crystalline and disordered structures. For the triangular lattice, the Poisson's ratio is identically unity and the shear modulus is identically zero. The nature of the potential allows for volume-preserving shear deformations to be made at zero temperature without energy cost. At temperatures where the harmonic approximation is valid, ground-state configurations have vanishing normal-mode frequencies. The fraction of vanishing frequencies increases with density and has a simple relation to χ for $\chi < 0.5$. At positive temperature,

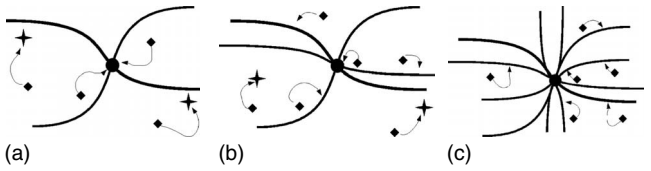

FIG. 15. Schematics of the energy landscape for (a) crystalline region $0.78 \leq \chi < 0.91$ $(0.0219 \leq \rho \leq 0.0253)$, (b) wavy-crystalline region and part of the disordered region, $0.50 \leq \chi < 0.78$ $(0.0253 < \rho \leq 0.0401)$, and (c) disordered region, $\chi < 0.5$ $(\rho > 0.0401)$. When minimizing the potential energy, initial configurations marked by the diamonds can fall by steepest-descent trajectories to the triangular lattice (center point), amorphous ground states (dark lines), or to local energy minima above the ground state (crosses). The heavy lines represent the ground-state manifolds running through the triangular lattice point.

these systems exhibit negative thermal expansion. When heated at constant density, the pressure attains a minimum and when heated at constant pressure, the system attains a density maximum.

These results are attributed to features of the energy landscape. At a density equal to ρ^*, the only global minima in the energy landscape are associated with the triangular lattice and its particle permutations. Upon compressing the system, additional global minima appear as "channels" running through the triangular lattice point. Further compression of the systems into the wavy-crystalline regime yields a significantly higher number of intersecting channels. Points in the energy landscape associated with Bravais lattices have a higher number of intersecting channels running through them than do amorphous ground-state configurations. This trend continues as the system is compressed further into the disordered region.

We have constructed a schematic of a projection of the energy landscape in Fig. 15. Diamonds represent initial conditions for steepest-descent trajectories for minimizing Φ and the arrows represent the trajectories down the energy landscape. The dark lines represent the ground-state manifolds intersecting at the central point associated with the triangular lattice. Crosses represent local minima that are higher in the energy landscape.

For the crystalline region, $0.78 \leq \chi < 0.91$, the energy landscape must be shaped in such a way to favor the triangular lattice over all other ground-state structures by nature of the relative size of the capture basin. The capture basin for a ground-state structure is the region of configurational space for which quenchings of the potential energy function by steepest-decent trajectories return to a specific structure [41]. In the crystalline region, the overall symmetry of the triangular lattice must be reflected in the topography of the energy landscape so as to give the triangular lattice the largest capture basin while other possible ground-state structures must have relatively much smaller capture basins. When using a perturbed triangular lattice as the initial condition for a minimization of the potential energy, the resulting configuration is either the triangular lattice or a local minimum of higher energy in the vicinity of the triangular lattice. These latter structures appear to be a triangular lattice with a vacancy or grain-boundary defect. Local minima typically arise when each particle is randomly perturbed by about 5% or more of the lattice spacing from its original site. Despite the existence of other Bravais-lattice configurations as ground states, the minimization routine has never found one. One must use infinitesimal perturbations from these Bravais lattices in order for the minimization routine to yield the ground state. In general, most random initial conditions lie within capture basins for local minima. This situation is shown schematically in Fig. 15(a) as configurations local to the triangular lattice point fall to the lattice point and all others result in local minima.

In the wavy-crystalline region, $0.58 \leq \chi < 0.78$. In Fig. 15(b), the nature of the capture basins changes significantly. Random configurations used as initial conditions for minimizations of the potential energy occasionally result in ground states, although usually they result in higher-energy local minima. In our experience, random initial conditions in this χ range have never resulted in a perfect triangular lattice ground state. Using a perturbed triangular lattice as an initial condition, random perturbations of each particle from its lattice site of less than 2% of the lattice spacing are large enough for the numerical minimization to find wavy-crystalline ground states. In general for this χ region, the capture basins for wavy-crystalline ground states dominate configurational space, even in the local vicinity of the triangular lattice point.

Upon further compression of the system into the disordered region, $\chi < 0.58$, disordered structures dominate the ground state manifold and the capture basins of Bravais-lattice structures are points of very small measure. Minimization of the potential energy does not result in the triangular lattice except for very small perturbations about the lattice point. More specifically, for $\chi < 0.5$, our minimization routine has not encountered a local minimum. With the energy landscape devoid of local minima for these χ, the ground state is the only outcome from steepest-descent trajectories.

A close look at these results, particularly the hysteresis studies via molecular dynamics, provides an interesting observation into the notion of glasses. Glasses are mechanically rigid, amorphous systems that have been rapidly quenched and as a result, the systems are kinetically trapped in local energy minima. Typically, glasses are metastable with respect to crystalline ground states. However, in the wavy-crystalline and disordered regions at zero temperature, most ground states are amorphous and all ground states tested above ρ^*, including the triangular lattice, are not mechanically rigid. There are vanishing normal-mode frequencies and the shear elastic constant is zero indicating a lack of internal restoring force. With the overlap potential, one wonders whether true glasses can be constructed upon rapid cooling considering that ground states are not mechanically rigid. In order to do so, the energy landscape must contain local energy minima above the ground-state energy without vanishing mode frequencies (aside from overall translation). To this point, rapid cooling of a system for certain densities produced hysteresis as T goes to zero, similar to that of Fig. 9 but done at constant density. The system is evidently stuck in a local energy minimum above the ground state. The extent of the hysteresis effect is dependent on χ and for $\chi < 0.5$, the hysteresis effect disappears. From our experience

with the numerical optimizations [17–20], the energy landscape likely does not contain local minima for $\chi<0.5$ as minimizations of the potential energy have always yielded ground states for these χ. Presumably the constraints on the $C(\mathbf{k})$'s are not sufficient in number to provide trapping in a local energy minimum. Future work will entail investigating this paradoxical phenomenon of producing rigid glasses with respect to nonrigid ground states. Additionally, given the lack of internal restoring forces in the ground state, a close examination of dynamic properties, including self-diffusion and shear viscosity, may uncover unusual transport properties.

By way of duality relations for classical ground states [2], there are direct connections between the ground-state energies of the overlap $V(k)$ and a real-space overlap $v(r)$ that has compact support at $r=1$. At the densities of interest, systems interacting via the overlap $V(k)$ are insensitive to the potential function much like systems interacting via a square mound $v(r)$ are insensitive to the potential function at low densities. However, the following distinction between the respective energy landscapes has to be made. For a square mound $v(r)$ or hard disks at low densities, the ground states are disordered and the corresponding portion of the energy landscape is a flat manifold walled in by positive energy or even forbidden configurations (overlapping disks). However, for the overlap $V(k)$, the energy landscape is a continuous hypersurface with many energetically degenerate manifolds sweeping throughout.

It is important to point out that the results in Sec. V hold for any potential whose $V(k)$ is bounded, positive, and has compact support at K for $d=2$. Since $V(k)$ is independent of structure, $C(\mathbf{k})$ is the only relevant quantity. Since these $V(k)$ share the same ground states for $\rho>2.19\times10^{-2}$, they also share the same $C(\mathbf{k})$. For a given χ, the fractions of modes with nonzero, real frequencies are identical for all $V(k)$ in this class. Additionally, because of the nature of the potential, similar macroscopic behavior should be expected. However, it is unclear whether the phase behavior of systems interacting via the overlap potential is similar to that of other $V(k)$ in the same general class. For instance, it is not known whether a linear ramp $V(k)$ would produce negative thermal expansion. Perhaps the form of $V(k)$ is amenable to a more mathematical analysis in determining positive-temperature phase behavior, but this approach has yet to be taken.

Lastly, the linear relation between the fraction of modes with nonzero, real frequencies and χ holds for $\chi<0.5$ for systems in dimensions one and three. Future work investigating the phase behavior of these spatial dimensions may uncover unusual behavior. Even in the first spatial dimension, an infinite number of ground-state "phase transitions" has been identified [2] but the thermal properties have yet to be explored. The nature of this class of soft, bounded potentials has been relatively unexplored, yet as we have shown here, the low-temperature behavior can be quite surprising.

ACKNOWLEDGMENTS

S.T. thanks the Institute for Advanced Study for its hospitality during his stay there. This work was supported by the Office of Basic Energy Sciences, U.S. Department of Energy, Grant No. DE-FG02-04-ER46108 and the National Science Foundation MRSEC Program under Award No. DMR-0820341.

[1] C. N. Likos, Phys. Rep. **348**, 267 (2001).
[2] S. Torquato and F. H. Stillinger, Phys. Rev. Lett. **100**, 020602 (2008).
[3] P. J. Flory and W. R. Krigbaum, J. Chem. Phys. **18**, 1086 (1950).
[4] F. H. Stillinger, J. Chem. Phys. **65**, 3968 (1976).
[5] F. H. Stillinger and T. A. Weber, J. Chem. Phys. **68**, 3837 (1978).
[6] F. H. Stillinger and T. A. Weber, J. Chem. Phys. **70**, 4879 (1979).
[7] A. Lang, C. N. Likos, M. Watzlawek, and H. Lowen, J. Phys.: Condens. Matter **12**, 5087 (2000).
[8] F. H. Stillinger and D. K. Stillinger, Physica A **244**, 358 (1997).
[9] C. E. Zachary, F. H. Stillinger, and S. Torquato, J. Chem. Phys. **128**, 224505 (2008).
[10] H. Cohn and A. Kumar, Phys. Rev. E **78**, 061113 (2008).
[11] C. Marquest and T. A. Witten, J. Physique **50**, 1267 (1989).
[12] R. D. Groot and P. B. Warren, J. Chem. Phys. **107**, 4423 (1997).
[13] C. N. Likos, H. Löwen, M. Watzlawek, B. Abbas, O. Jucknischke, J. Allgaier, and D. Richter, Phys. Rev. Lett. **80**, 4450 (1998).
[14] A. Sütő, Phys. Rev. Lett. **95**, 265501 (2005).
[15] F. H. Stillinger, Phys. Rev. B **20**, 299 (1979).
[16] F. H. Stillinger, Phys. Rev. E **66**, 066125 (2002).
[17] Y. Fan, J. K. Percus, D. K. Stillinger, and F. H. Stillinger, Phys. Rev. A **44**, 2394 (1991).
[18] O. U. Uche, F. H. Stillinger, and S. Torquato, Phys. Rev. E **70**, 046122 (2004).
[19] O. U. Uche, S. Torquato, and F. H. Stillinger, Phys. Rev. E **74**, 031104 (2006).
[20] R. D. Batten, F. H. Stillinger, and S. Torquato, J. Appl. Phys. **104**, 033504 (2008).
[21] S. Torquato, Soft Matter **5**, 1157 (2009).
[22] S. Torquato and F. H. Stillinger, Phys. Rev. E **68**, 041113 (2003).
[23] We use the phrase "non-Bravais lattice" to refer to periodic structures with a multiparticle basis.
[24] R. D. Batten, F. H. Stillinger, and S. Torquato, Phys. Rev. Lett. **103**, 050602 (2009).
[25] A. Sütő, Phys. Rev. B **74**, 104117 (2006).
[26] J. B. Hooper, K. S. Schweizer, T. G. Desai, R. Koshy, and P. Keblinski, J. Chem. Phys. **121**, 6986 (2004).
[27] N. W. Ashcroft and N. D. Mermin, *Solid State Physics* (Saunders College Publishing, Philadelphia, 1976).

[28] L. Brillouin, *Wave Propagation in Periodic Structures* (Dover Publications, New York, 2003).
[29] L. D. Landau and E. M. Lifshitz, *Theory of Elasticity* (Butterworth-Heinemann, Boston, 1995).
[30] M. C. Rechtsman, F. H. Stillinger, and S. Torquato, Phys. Rev. Lett. **101**, 085501 (2008).
[31] L. Verlet, Phys. Rev. **159**, 98 (1967).
[32] H. C. Andersen, J. Chem. Phys. **72**, 2384 (1980).
[33] We have also used rhombical simulation cells allowing for the perfect triangular lattice. Additionally, for *NPT* simulations, we allowed the simulation cell to deform and we observed no significant differences in equilibrium properties between this and the square simulation box.
[34] K. H. Chow and D. M. Ferguson, Comput. Phys. Commun. **91**, 283 (1995).
[35] H. J. C. Berendsen, J. P. M. Postma, W. F. van Gunsteren, A. DiNola, and J. R. Haak, J. Chem. Phys. **81**, 3684 (1984).
[36] M. C. Rechtsman, F. H. Stillinger, and S. Torquato, J. Phys. Chem. A **111**, 12816 (2007).
[37] B. M. Mladek, P. Charbonneau, C. N. Likos, D. Frenkel, and G. Kahl, J. Phys.: Condens. Matter **20**, 494245 (2008).
[38] C. N. Likos, A. Lang, M. Watzlawek, and H. Löwen, Phys. Rev. E **63**, 031206 (2001).
[39] H. Fragner, Phys. Rev. E **75**, 061402 (2007).
[40] C. N. Likos, B. M. Mladek, D. Gottwald, and G. Kahl, J. Chem. Phys. **126**, 224502 (2007).
[41] F. H. Stillinger and T. A. Weber, Phys. Rev. A **25**, 978 (1982).